

# Simulating a metallicity-dependent initial mass function: Consequences for feedback and chemical abundances

Thales A. Gutcke<sup>1\*</sup> and Volker Springel<sup>2,3,4</sup>

<sup>1</sup>Max-Planck-Institut für Astronomie, Königstuhl 17, 69117 Heidelberg, Germany

<sup>2</sup>Heidelberg Institute for Theoretical Studies, Schloss-Wolfsbrunnengasse 35, 69118 Heidelberg, Germany

<sup>3</sup>Zentrum für Astronomie der Universität Heidelberg, ARI, Monchhofstrasse 12-14, D-69120 Heidelberg, Germany

<sup>4</sup>Max-Planck-Institut für Astrophysik, Karl-Schwarzschild-Str. 1, D-85748, Garching, Germany

26 November 2018

## ABSTRACT

Observational and theoretical arguments increasingly suggest that the initial mass function (IMF) of stars may depend systematically on environment, yet most galaxy formation models to date assume a universal IMF. Here we investigate simulations of the formation of Milky Way analogues run *ab initio* with an empirically derived metallicity-dependent IMF and the moving-mesh code AREPO in order to characterize the associated uncertainties. In particular, we compare a constant Chabrier and a varying metallicity-dependent IMF in cosmological, magneto-hydrodynamical zoom-in simulations of Milky Way-sized halos. We find that the non-linear effects due to IMF variations typically have a limited impact on the morphology and the star formation histories of the formed galaxies. Our results support the view that constraints on stellar-to-halo mass ratios, feedback strength, metallicity evolution and metallicity distributions are in part degenerate with the effects of a non-universal, metallicity-dependent IMF. Interestingly, the empirical relation we use between metallicity and the high mass slope of the IMF does not aid in the quenching process. It actually produces up to a factor of 2-3 more stellar mass if feedback is kept constant. Additionally, the enrichment history and the  $z = 0$  metallicity distribution are significantly affected. In particular, the alpha enhancement pattern shows a steeper dependence on iron abundance in the metallicity-dependent model, in better agreement with observational constraints.

**Key words:** galaxies: formation – stars: mass function – methods: numerical

## 1 INTRODUCTION

The majority of stars are known to form in shared star formation (SF) regions known as embedded clusters (Lada & Lada 2003; Kroupa et al. 2005; Megeath et al. 2016). The cause of this is assumed to be the collapse of giant molecular clouds (GMC) where many stars form simultaneously. This implies a distribution of stellar masses originating from each collapse, the stellar initial mass function (IMF). An unanswered question in stellar and galaxy formation physics is whether the IMF is universal, i.e. whether the distribution is the same in each star forming region or varies systematically with some dependency on its environment.

The details of the physics governing the regulation of star formation are poorly understood, since it is still unclear to what degree radiation, turbulence, magnetic fields,

and instantaneous feedback from the forming young stars are able to counteract a pure gravitational collapse model. But observations of the Milky Way (MW) Galaxy, including resolved imaging of individual stars in globular clusters and the use of dwarf and giant sensitive spectral features, are broadly in agreement with a universal IMF shape in the MW (Scalo 1986; Kroupa 2001; Chabrier 2003; Bastian et al. 2010; Hopkins 2013). Pioneering observational work on the IMF and a first functional fitting form were made by Salpeter 1955, who suggested a power law slope of 1.35. Later, Kroupa (2001) and Chabrier (2003) added a low mass turn over to this basic model.

Studies of other galaxies yielded varying results. Some are consistent with the results from the MW (Kroupa 2002; Chabrier 2003; Kirk & Myers 2011; Bastian et al. 2011). But Larson (1998) showed that most observations are compatible with a moderate IMF variation in time. For example, both the G-dwarf problem and the large amount of heavy elements in clusters can be reconciled with a change by

\* thales@mpia.de

a factor of  $\sim 3$  in the dwarf-to-giant ratio. Recently, further evidence for IMF variations has emerged, especially in early-type galaxies (e.g. [Hoversten & Glazebrook 2008](#); [Meurer et al. 2009](#); [Gunawardhana et al. 2011](#); [Conroy & van Dokkum 2012](#); [Cappellari et al. 2013](#)). Studying resolved star clusters in M31, [Weisz et al. 2015](#) found a steeper high-mass power law slope of  $(1.45 \pm 0.05)$ . [Martín-Navarro et al. \(2015\)](#) used a sample of CALIFA elliptical galaxies to demonstrate a dependency of the IMF on the metallicity of the gas from which the stars formed. They use the dwarf-to-giant ratio and allowed the high-mass slope,  $\Gamma_b$ , of the Vazdekis IMF ([Vazdekis et al. 1996](#)) to vary.

Since compact ETGs are believed to be stellar dominated at their centers, one way of measuring the IMF of integrated light is to use the mass-to-light ratio as a proxy for the fraction of low-mass stars (e.g. [Dutton et al. 2011](#)). Using this method, [Conroy et al. \(2013\)](#) analyze a sample of compact elliptical galaxies and find IMF variations with velocity dispersion ( $\sigma$ ). They show that galaxies with  $\sigma \sim 100$  km s<sup>-1</sup> have IMF slopes most similar to the Milky Way. Intermediate velocity dispersion galaxies ( $\sigma \sim 160$  km s<sup>-1</sup>) become more bottom-heavy, with an IMF shape best fit by a Salpeter IMF. The highest velocity dispersion galaxies with  $\sigma \sim 250 - 300$  km s<sup>-1</sup> have yet more bottom-heavy IMFs. [La Barbera et al. \(2013\)](#) attempt to put constraints on the IMF using a large spectroscopic sample of early-type galaxies from the SPIDER survey. They also find a correlation between the IMF slope  $\Gamma$  and the central velocity dispersion. A similar result is obtained by [Spiniello et al. \(2014\)](#), who use a set of galaxies from the MILES library of stellar spectra to show a dependency of the IMF slope on the global velocity dispersion.

[Chabrier et al. \(2014\)](#) examine the evidence in the literature supporting a variable IMF in “extreme starburst environments” and in massive early-type galaxies (ETGs). They show that ETGs sport spectral absorption features, larger mass-to-light ratios and larger  $[\alpha/\text{Fe}]$  than spiral galaxies. ETGs therefore are assumed to host more low-mass stars such as M dwarfs. The authors postulate that these local ETGs evolved from small, compact dense progenitors between  $z \sim 3 - 5$ . These very compact systems were  $10^3$  times denser than the Milky Way (MW), had higher velocity dispersions and possibly higher temperatures. Also, these progenitors had different turbulent velocity than the MW, producing intense pressure and high accretion rates. The IMF in these “extreme starburst environments” is thus expected to be bottom-heavy with respect to the MW.

Simulations have also been used to study the effect of an IMF variation on the properties of galaxies. [Blancato et al. \(2017\)](#) post-process the Illustris simulation to study the effects of an IMF dependency on local and global velocity dispersion and on the metallicity, finding that the hierarchical nature of massive galaxy assembly significantly complicates the interpretation of the observed trends.

[Yan et al. \(2017\)](#) build on the integrated galactic IMF (IGIMF) model ([Kroupa & Weidner 2003](#)). This model defines the galaxy-wide IMF as the integration of both the local IMF of a single embedded star cluster and the cluster mass function. Smaller clusters can be “optimally sampled” from a universal local IMF, but given their total mass, will not produce any stars more massive than the cluster mass.

The result for galaxies as a whole is that a universal local IMF can produce a IGIMF that varies.

[Clauwens et al. \(2016\)](#) also use the metallicity-dependent IMF from [Martín-Navarro et al. \(2015\)](#), applying it to a sample of SDSS galaxies to investigate the effect on total stellar mass and star formation rates. They find that a bottom-heavy IMF at late times can aid in the quenching process, speeding it up. [Guszejnov et al. \(2017\)](#) use the FIRE simulation suite to study the IMF variation caused by a number of different cloud collapse models, and show that only a protostellar feedback model produces small enough variations to be consistent with observations.

This paper is organised as follows. Section 2 recaps the simulation code and physics, Section 3 describes the variable IMF model, Section 4 compares the Chabrier and variable IMF results, and Section 6 summarises our findings. We use the cosmological parameters from the most recent Planck results ( $\Omega_m = 0.31$ ,  $\Omega_L = 0.69$ ,  $\Omega_b = 0.0486$ ,  $h = 0.677$ ,  $\sigma_8 = 0.8159$ ,  $n_s = 0.97$  [Planck Collaboration et al. 2016](#)). We assume solar metallicity,  $Z_\odot$ , to be 0.0127. We use the variables  $R_{\text{crit},200}$  and  $R_{\text{vir}}$  interchangeably to denote the radius inside which the average density is 200 times the critical density.

## 2 NUMERICAL SIMULATIONS

We have run six zoom-in simulations of Milky Way mass galaxies ( $\sim 10^{12} M_{\text{crit},200}$  at  $z = 0$ ). The initial conditions are drawn from the Auriga zoom-in simulation project presented in [Grand et al. \(2017b\)](#), and correspond to their galaxy numbers 6, 9, 13, 16, 24, and 28. We use the magneto-hydrodynamical moving-mesh code AREPO ([Springel 2010](#)) with a physics setting that differs slightly from the Auriga project with respect to parameters used for black hole seeding, active galactic nuclei feedback, and galactic winds. In particular, we use here the updated yield tables introduced in the IllustrisTNG simulation ([Pillepich et al. 2017](#); [Naiman et al. 2017](#)) project. These changes in the details of the physics implementation with respect to Auriga are however immaterial for the qualitative results of our simulations. Nevertheless, to differentiate the true Auriga galaxies from our re-simulations also in the universal IMF case (which have slightly different physics), we will henceforth call our galaxies “Halo-X”, where ‘X’ denotes the corresponding number 6, 9, 13, 16, 24 and 28 in the Auriga project.

The IMF slope effects both the SNII rate and the AGB wind metal enrichment. The SNII rate at a given timestep is determined by

$$N_{\text{SNII}}(t, \Delta t) = \int_{M_{\text{low}}}^{M_{\text{high}}} \Phi(m) dm. \quad (1)$$

For SNII,  $M_{\text{low}} = \max[M(t + \Delta t), 8 M_\odot]$  and  $M_{\text{high}} = \min[M(t), 100 M_\odot]$ , where  $M(t, Z)$  is the inverted stellar lifetime function (see [Vogelsberger et al. 2013](#), section 2.3.1). The yields for AGB stars are taken from [Karakas \(2010\)](#) for  $1 - 6 M_\odot$ , and from [Doherty et al. \(2014\)](#) and [Fishlock et al. \(2014\)](#) for  $7 - 7.5 M_\odot$ . The SNII yields are taken from [Portinari et al. \(1998\)](#) for  $6 - 13 M_\odot$  and  $40 - 120 M_\odot$ . For  $13 - 40 M_\odot$ , they are from [Kobayashi et al. \(2006\)](#).

The mass fraction of SNIa (in the range  $1.4 - 8 M_\odot$ ) for different IMF is not changed in our model. Likewise, the

“delay time distribution” function,  $g(t)$ , is taken in unmodified form from the Pillepich et al. (2017) model. Since the binary fraction and the time delay distribution of SNIa are very uncertain, we did not attempt to couple them to the variable IMF model. We make this choice for consistency, because the fiducial model assumes them to be fixed and independent of the IMF.

The SNIa rate is nevertheless indirectly affected by the changed star formation history. It is computed as

$$\dot{N}_{Ia}(t) = \int_0^t \Psi(t')g(t-t') dt', \quad (2)$$

where  $\Psi(t')$  is the star formation rate and  $g(t-t')$  is the delay time distribution (DTD) defined as

$$g(t) = \begin{cases} 0 & \text{if } t < 40\text{Myr} \\ N_0 \left( \frac{t}{40\text{Myr}} \right)^{-s} \frac{s-1}{40\text{Myr}} & \text{if } t \geq 40\text{Myr}, \end{cases} \quad (3)$$

The SNIa yields are taken from Nomoto et al. (1997).

The fiducial resolution level of the bulk of our simulations corresponds to “level 5” as tabulated in Grand et al. (2017b). We also run one “level 4” version of Auriga halo number 16 as a resolution test. The fiducial baseline IMF when universality is assumed is the Chabrier IMF (Chabrier 2003), which we compare with a simple metallicity-dependent IMF model described in the following section.

### 3 THE VARIABLE IMF MODEL

We use the relation derived in the study by Martín-Navarro et al. (2015) as the starting point of our simulations. The relation presented in Martín-Navarro et al. (2015) is interesting to explore because it is a recent study and because metallicity is a very plausible candidate for IMF variations from a theoretical perspective. Since this study is intended as an initial exploration, we leave the other empirical relations presented in the literature (e.g. Hoversten & Glazebrook 2008; Meurer et al. 2009; Gunawardhana et al. 2011; Marks et al. 2012) for future work.

The empirically derived relation between the high-mass slope of a Vasdekis IMF,  $\Gamma_b$ , and the  $[M/H]$  of the gas in Martín-Navarro et al. (2015) is:

$$\Gamma_b = 2.2(\pm 0.1) + 3.1(\pm 0.5) \times [M/H]. \quad (4)$$

We use this relation, but combine it with the Kroupa IMF (Kroupa 2001) to define a metallicity dependent IMF as follows:

$$\Phi(m) \propto \begin{cases} m^{-0.3} & \text{for } 0.1 < m/M_\odot < 0.5 \\ m^{-\Gamma_b} & \text{for } 0.5 < m/M_\odot < 100. \end{cases} \quad (5)$$

The integral of the IMF is normalised to the total initial stellar mass of a star particle,  $M_{\text{init}}$ . This mass has a resolution-dependent target value corresponding to our gas-cell resolution but can vary slightly around the target value as described in Vogelsberger et al. (2013). We extract the value for  $[M/H]$  from the simulation as

$$[M/H] = \log_{10} \left( \frac{\sum \frac{M_Z}{M_{\text{tot}}}}{Z_\odot} \right), \quad (6)$$

MNRAS 000, 1–9 (—)

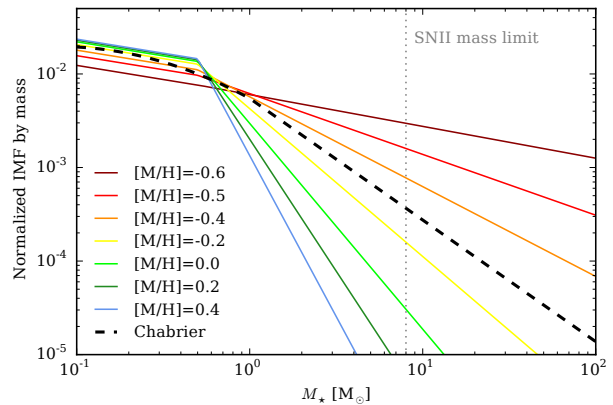


**Figure 1.** Illustration of the varying IMF (by mass) with different  $[M/H]$  values. The dashed black line is the Chabrier IMF. The grey dotted line indicates the lower mass limit for core collapse supernovae.

summing over all  $Z$  above He.

In the following, we will use the terms “bottom-heavy” and “top-heavy” to refer to IMFs with large and small (or even negative)  $\Gamma_b$ , respectively. Given that each IMF is re-normalized to  $M_{\text{init}}$ , a steep high-mass slope will leave more stellar mass in the low-mass region. Thus, these terms only refer to the relative amount of  $M_{\text{init}}$  in the low-mass ( $\lesssim 1 M_\odot$ ) and high-mass ( $\gtrsim 1 M_\odot$ ) regions of the IMF.

Since the observations of IMF variations are as of yet inconclusive, the common choice made by most galaxy formation simulations is to assume universality (an Occam’s razor argument). The primary goal of our present analysis is to assess the magnitude of potential changes in global galaxy properties that a variable IMF consistent with observations can produce. This then provides an approximate determination of the uncertainties associated with making the ad-hoc choice of a universal IMF.

Most simulations studying variable IMF models use simulations run with a constant IMF and post-process these to re-calculate galaxy properties assuming a variable IMF. These models cannot easily account for the non-linear effects caused by variability, i.e. for the changes in star formation rates and associated feedback resulting from variations in the enrichment history due to a different IMF. Thus, a second goal of our analysis is to understand such non-linear effects on the metallicity that a variable IMF can cause. Hence, we will investigate the enrichment history and the metallicity distribution functions (MDFs) of our simulated galaxies.

We note that Martín-Navarro et al. (2015) used early type galaxies to derive their empirical relation, whereas our study focuses on Milky Way-like spiral galaxies. While there is no direct evidence that the relation also applies to late type galaxies, we here shall assume that it does. We make this simplifying assumption mainly because the Milky Way is the most important Galaxy for chemo-dynamical studies. Examining other galaxy mass regimes is beyond the scope of this paper. Conceptually, this also means that only one new parameter (in our case the metallicity of the star-forming gas) is added when moving from the assumption of a

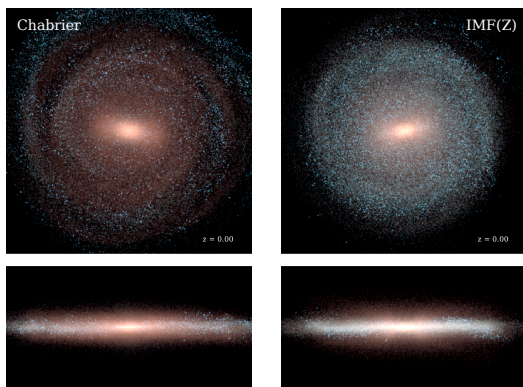


**Figure 2.** RGB images of Halo 16 for Chabrier IMF (left) and the metallicity dependent IMF (right). The galaxy is rotated to see the disk face-on in the upper panels, and edge-on in the lower panels. The images are 50kpc wide. The K-, B-, and U-filters were mapped to RGB channels, respectively. We note that the photometric calculations assume a Chabrier IMF in both cases.

fixed universal IMF to a universally varying IMF. This thus represents the next simplest model in which the variation of the IMF with metallicity is identical in all types of galaxies.

## 4 RESULTS

### 4.1 Stellar mass evolution

Given the mutual self-regulated coupling of star formation and stellar feedback it is difficult to predict a priori whether our variable IMF simulations would produce more or less stellar mass than their Chabrier counterparts. Since metallicity is low at early times, the IMF in our model has a shallow slope then (being “top-heavy”), allowing for many high mass stars. These in turn produce a lot of core-collapse supernovae (SNII) and stellar feedback. The heating from the feedback can inhibit further star formation. On the other hand, the increase in high mass stars at early times also produces significant early enrichment in the gas. This enrichment steepens the IMF slope of subsequent generations of stars, thus decreasing the amount of feedback energy affecting the gas in subsequent cycles. A critical question then is, how long does it take to enrich the gas sufficiently that the IMF is truncated below  $8M_{\odot}$ , the minimum mass of core-collapse supernovae. Once this occurs, both chemical enrichment and stellar feedback come largely to a halt. Since our IMF variations do not affect the total mass of a formed star particle but only the distribution of its mass (the mass function), stellar mass build up can then proceed without the effect of feedback, due to the lack of high mass stars, and is solely regulated by the available gas reservoir after this point.

A bottom-heavy IMF and the resulting lack of stellar feedback has the further effect that less mass is returned to the interstellar medium (ISM) and becomes again available for subsequent star formation. Depending on the precise dependency of the IMF slope with metallicity, and on the efficiency of stellar feedback, these two processes can dominate at different times in a galaxy’s life.

Figure 2 shows  $z = 0$  RGB images of Halo 16 in face-on and edge-on projections for both our models. The RGB

channels use the K-, B- and U-filters based on the stellar population synthesis model by Bruzual & Charlot (2003). We note however that the image was created with the standard photometric calculation that assumes a Chabrier IMF, for simplicity. Thus, young stars (blue) are a bit brighter than they would self-consistently appear if the variable IMF was also used for making the image, since the variable model produces a bottom-heavy IMF at late times.

Figure 3 gives an overview of the stellar mass evolution of our six halos. The black solid line is the evolution with the universal Chabrier IMF, while the red line is the variable IMF model. The dotted lines show Halo 16 at resolution level 4. In all cases, the variable IMF model produces more stellar mass at early times ( $z \sim 2 - 3$ ) and keeps the lead for the entire evolution. The final stellar mass is a factor of 2-3 higher for the variable model in all model galaxies.

We stress that the feedback model was calibrated for the universal IMF and no adjustments were made to account for the variable IMF scenario. Thus, we do not claim that the variable IMF model alone can explain the observations. Instead, the change in final stellar mass should only be interpreted as a relative change from model to model when only the IMF parameterisation is changed, but other aspects of the model are left unchanged. Of course, if the variable IMF model was adopted as a new default description of the galaxy formation physics, the feedback strength would have to be re-calibrated. Increasing the feedback would likely again be able to match the stellar mass – halo mass relation.

Figure 3 shows the star formation histories of our six halos. The star formation rates are higher at early times in the variable IMF case, but drop below the Chabrier model in all but one of our halos by  $z = 0$ . Due to the shortage of core-collapse SN after  $z \sim 3$ , the gas in the galaxy becomes calm and is not driven into outflows. Thus, it is consumed by SF quickly at that time. The stars formed have a bottom heavy IMF that stores much of the mass for times close to the Hubble time. Thus, SF then decreases, in most cases below the Chabrier level.

### 4.2 Metallicity evolution

Stellar metallicity is what determines the IMF and subsequent evolution of each star particle. This is where the two IMF models show their most significant differences. The evolution of the total stellar metallicity of each halo is shown in Figure 3. The blue line and error bars are the binned MW data compilation from Mollá et al. (2015). All six halos in the variable model increase their global metallicity dramatically in the first 2 Gyr. After that, the evolution flattens out and stays practically constant for the last 8 Gyr till  $z = 0$ . The compiled observations from Mollá et al. (2015) allow for such a rapid increase at early times. But by  $z = 0$ , the Chabrier value better matches the data.

The gas phase metallicity evolution across the entire halo is shown in Figure 3 and sports the same change from Chabrier IMF to variable model. The total gas metallicity increases faster and earlier in the metallicity dependent case, and then slows its evolution, until no significant increase in total metallicity happens in the last 7-8 Gyr.

This similar trend in both the stellar and gas metallicity in the variable model can be explained by the change in IMF slope across time. Initially, the gas has a primordial



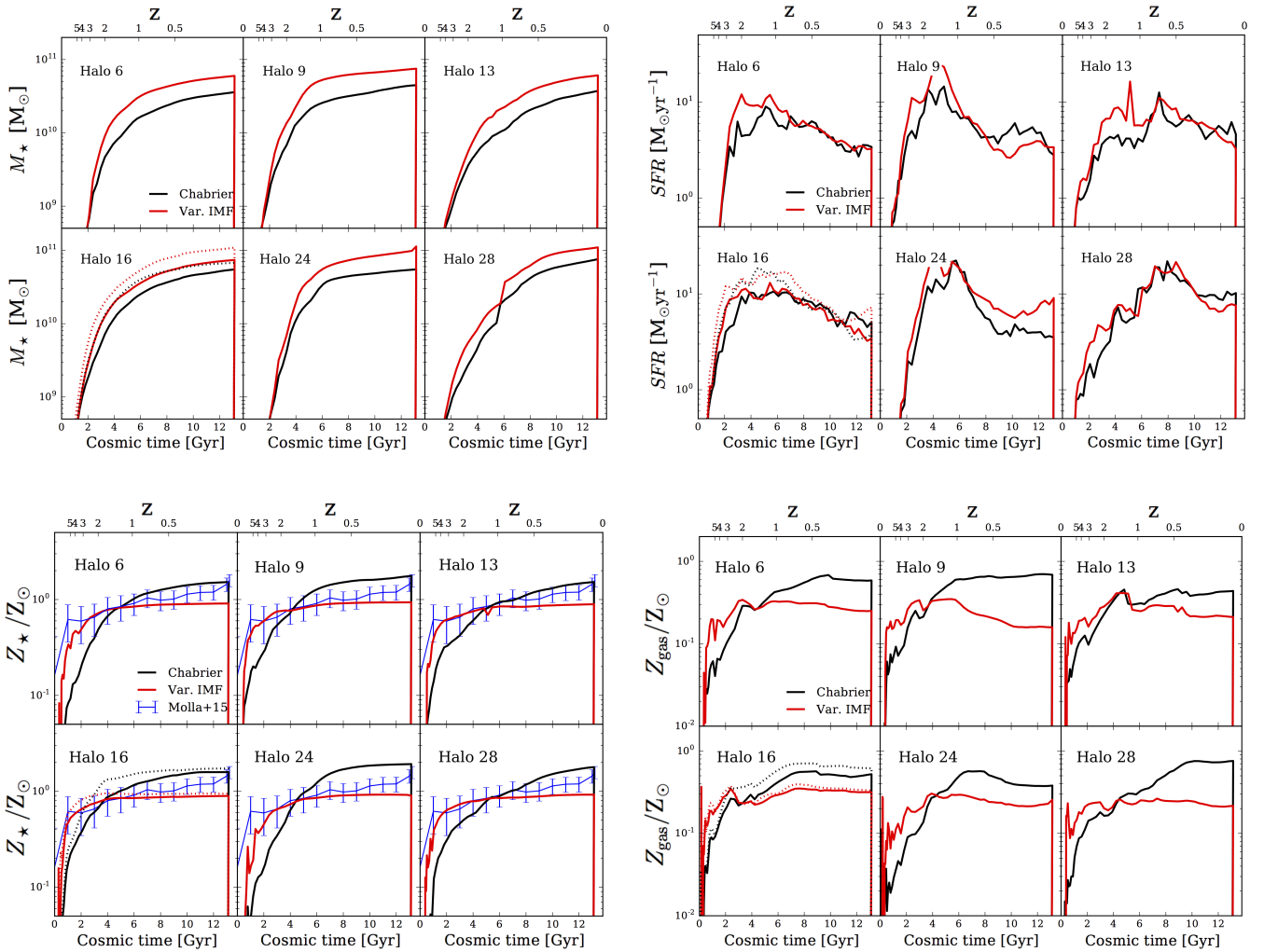


**Figure 3.** *Upper panels:* Stellar mass evolution (left) and star formation histories (right) for the six halos (initial conditions from the Auriga galaxies 6, 9, 13, 16, 24, 28). The black lines are the galaxies assuming a universal Chabrier IMF. The red lines are the same galaxies re-simulated with the metallicity-dependent IMF. The stellar mass is the sum of all star particle masses inside  $R_{\text{crit},200}$  at each timestep. The dotted lines in the panel with Halo 16 are the higher resolution versions of the same initial conditions. *Lower panels:* Total stellar (left) and gas (right) metallicity evolution of all stars within  $R_{\text{crit},200}$  for each galaxy. Lines are the same as in Figure 3. The blue error bars are the data points from Mollá et al. (2015), who compiled a variety observational studies of the Solar neighbourhood.

composition, with no metals. Thus, the IMF allows for many high-mass stars that undergo core collapse within the first 1-2 Gyr. This increases the metallicity rapidly. After this first phase, the gas has been enriched and the subsequent generation of stars have IMFs with much steeper slopes and fewer high-mass stars. The strong enrichment stops and the metallicity of both gas and stars does not increase much further.

In Figure 4, we compare our galaxy stellar metallicity to the observational data from Gallazzi et al. (2005) who used SDSS data. We match the observational selection by cutting the view at 5 kpc, which is the average physical size of the galaxies inside the SDSS fiber. The points show the ten most massive (and resolved) galaxies/satellites for each simulation. We compare Chabrier, Kroupa, Salpeter and variable IMF models. At low masses, we have added the MW satellite data from Kirby et al. (2010). At these low masses ( $M_{\text{crit},200} < 10^8 M_{\odot}$ ), the universal IMF models match the data better. Interestingly, at higher masses (the highest being the MW-like galaxy itself), the results for the metallicity-

dependent IMF are closer to the mean of the Gallazzi et al. (2005) data.

### 4.3 Metallicity distribution functions

The metallicity distribution functions (MDFs) of the stars and gas are a good way to track the changes caused by the variable IMF model, since the metallicity dependence causes non-linear effects in the metal production. The stellar MDFs are shown in Figure 5. Both models produce distributions that peak around  $[M/H] \simeq 0.0$ , but the variable IMF model is distributed less towards high metallicity. This is caused by the lack of high-mass stars at late times, since the IMF drops off steeply. In both cases the majority of metals are produced in core-collapse supernovae (SNII, dashed lines). In the Chabrier case, asymptotic giant branch stars (AGB) produce most of the remaining metals whereas SNIa contribute very little. In the variable IMF model, AGB and SNIa produce approximately the same amount.

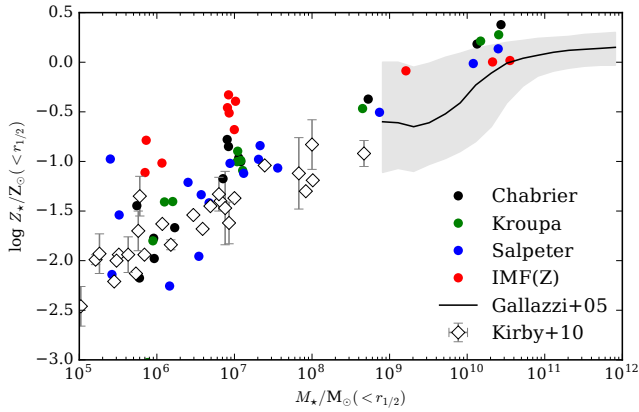


**Figure 4.** Stellar metallicity within the half mass radius,  $r_{1/2}$ , as a function of stellar mass. Dots represent the ten most massive halos/subhalos in the zoom simulation Halo 16. Three universal IMFs (Chabrier, Kroupa and Salpeter) and the metallicity dependent IMF are shown. The gray band shows the SDSS data from Gallazzi et al. (2005). Gray data with error bars show the MW dwarfs from Kirby et al. (2010).

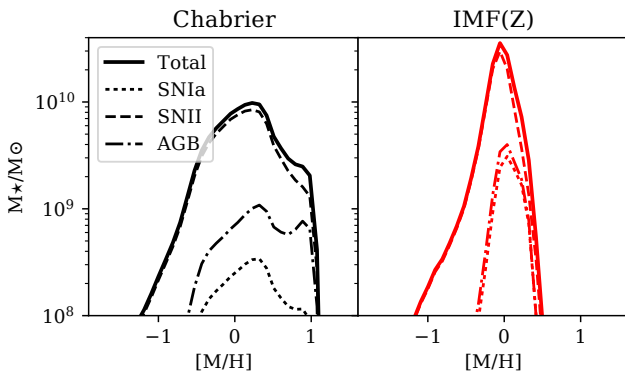


**Figure 5.** Stellar metallicity distribution function (solid line), split into contributions from SNIa (dotted), SNII (dashed) and AGB stars (dot-dashed). Shown is the  $z = 0$  simulation output of Halo 16 (level 4).

Model	m	$y_0$	$m_A$	$y_{0,A}$
Chabrier	-0.21	0.36	-0.15	0.30
IMF(Z)	-0.77	0.02	-0.79	-0.09

**Table 1.** Fit parameters for the  $[\alpha/\text{Fe}] - [\text{Fe}/\text{H}]$  relation with the linear function  $[\alpha/\text{Fe}] = m \cdot [\text{Fe}/\text{H}] + y_0$ . The fit parameters for the data after the APOGEE selection function are also shown, indicated by the index A.

#### 4.4 $\alpha$ -Enhancement

The so-called  $\alpha$ -enhancement is an important independent constraint on simulations. It has often been disregarded in the comparison with observations since it is difficult to match and depends on many factors in the simulations. In

particular, it depends not only on the IMF, but also on the prescription for SNIa, the ratio of SNIa to SNII and, importantly, the yield sets used.

Marinacci et al. (2014) previously explored the  $\alpha$ -abundance patterns predicted in AREPO simulations, finding a need to increase the SNIa rate by a factor of  $\sim 4$  and being prompted to add fully metal-loaded winds to reproduce the slope of the observations. For a study of the  $\alpha$ -abundances of the Auriga sample, see Grand et al. (2017a). We show the  $[\alpha/\text{Fe}] - [\text{Fe}/\text{H}]$  plane in Figure 6. Our estimate of  $\alpha$  is calculated by averaging the metallicity contribution of oxygen, silicon and magnesium.

To compare our simulations with the Milky Way, we show data from the SDSS Apache Point Observatory Galactic Evolution Experiment (APOGEE), which is a high-resolution near-infrared spectroscopic survey (first presented in Bovy et al. 2014). The chemical abundances were updated to a homogeneous sample by Ness et al. (2017). We choose stars in the radial range  $5 < R_{\text{GC}}/\text{kpc} < 9$ , where  $R_{\text{GC}}$  is the distance to the Galactic center in the plane of the disk. The scale height is confined to  $|z|/\text{kpc} < 1$ . APOGEE uses red clump stars and these have a strong age-dependent selection function, described in Bovy et al. (2014, their equation 11). We mimic this selection function when analysing the simulation data, which is strongly biased towards young stars.

The left panels show the data for Chabrier, and the right ones for the metallicity dependent IMF. The colored images display the distribution of the simulation, while the overplotted black contours show the APOGEE data. The graphs to the top and sides are the one-dimensional histograms of the same data. Here the simulations are shown as red dashed lines, while APOGEE is given through black solid lines. The variable IMF model causes a significant change in the  $\alpha$  enhancement of the stars. The distribution becomes much steeper and the mean matches the data better. The shape and slope of the distribution in the Chabrier model seem to match the data more closely, but in this case the normalization is off by around 0.3 dex. We fit the slope of the  $[\alpha/\text{Fe}] - [\text{Fe}/\text{H}]$  distribution with and without the APOGEE selection function. The fit results are noted in Table 1. In the Chabrier case, the selection function causes the fit to be shallower, the slope being 0.21 without and 0.15 with it. This is opposite in the variable IMF case, where the slope becomes 0.79 with the age selection and 0.77 without.

We note that the bimodality in  $[\alpha/\text{Fe}]$  of the Chabrier model is likely due to the age-selection, since the total distribution in the simulation does not show this trend. We assume that the overlapping functional forms of the SFH (which peaks at  $z \sim 2$ ) and the age-dependent selection function (which peaks around  $z \sim 0.15$ ) can cause an apparent dip in the distribution, making it seem bimodal. Our IMF(Z) model does not show a bimodal trend in  $[\alpha/\text{Fe}]$ . As Grand et al. (2017a) have shown, the occurrence of the bimodality in simulations is very dependent on the SFH and can also be hidden in some systems. The altered SFH in the variable model may thus well account for the lack of a bimodality. Additionally, it is possible that this result is sensitive to the specific SNIa prescription that is used.

In Figure 7, we show the  $[\text{Fe}/\text{H}]$  distribution of stars in the entire halo. The dashed and dotted lines are the components of the distribution split by the channel in which the iron was produced. In the Chabrier model, SNIa and

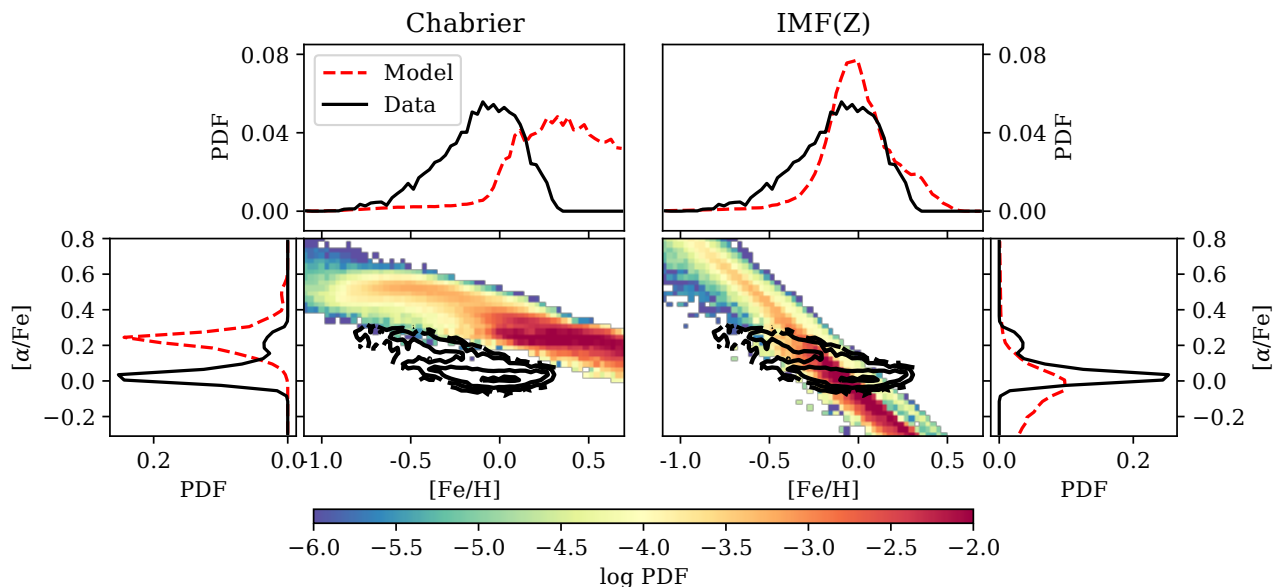


**Figure 6.** Distribution of simulated stars in the  $[\alpha/\text{Fe}]$  vs  $[\text{Fe}/\text{H}]$  plane for Chabrier (left panels) and metallicity-dependent IMF (right panels). The black contours are the APOGEE data (Bovy et al. 2014; Ness et al. 2017). We attempt to mimic the age selection function of APOGEE. The spatial selection for both the model and APOGEE is the following:  $5 < R_{\text{xy}}/\text{kpc} < 9$  and  $|z|/\text{kpc} < 1$ . The bin width is set to 0.05 in abundance space for both axes. Shown is the  $z = 0$  simulation result of Halo 16 (level 4).

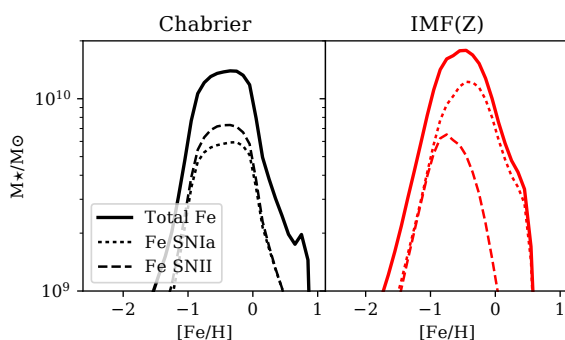


**Figure 7.** Distributions of  $[\text{Fe}/\text{H}]$  for Chabrier and metallicity-dependent IMF. Dotted lines show the iron component created in SNIa. Dashed lines show the iron from SNII. Displayed is the  $z = 0$  simulation result of Halo 16 (level-4 resolution).

SNII produce approximately equal amounts of iron. In the variable IMF model, most of the metal-rich stars have their iron from SNIa alone. This difference in iron production is the driving factor that changes the  $\alpha$ -enhancement between the two models. The increased iron production at late times (and high metallicity) brings the  $[\alpha/\text{Fe}]$  ratio down to solar values and causes the steep dependence in the distribution.

## 5 DISCUSSION

This study differs significantly from previous work studying a variable IMF in simulations since it implements the IMF variability *ab initio* rather than in post-processing and introduces only a single additional parameter. This allows a detailed analysis of the non-linear effects of both the metallicity enrichment and the amount of feedback generated by the changing IMF across time. Additionally, it is a study of

how the IMF may vary within a single galaxy rather than across the galaxy population.

One study that examines the effects of different IMFs on individual galaxies is the work by Few et al. (2014). They test three universal IMFs (the models presented in Salpeter 1955; Kroupa et al. 1993; Kroupa 2001) by running multiple manifestations of a simulated  $L^*$  galaxy. They note that more top-heavy IMFs are more efficient at forming stars and attribute this to the strong replenishment of gas caused by the larger fraction of high-mass stars. Although this study does not include a varying IMF, it nevertheless exhibits some of the same features as our work. At earlier times, when the metallicity is still low and the IMF still top-heavy in our simulations, the SFR is also higher due to the large amount of gas injected into the ISM from the increased number of supernovae. And yet, in our varying model the SFR drops after this initial burst, since the increased supernovae drive metal enrichment and, thus, more bottom-heavy IMFs in the subsequent cycle of star formation.

Possibly the most similar study to ours is by Bekki (2013). They implement *ab initio* IMF slopes that are allowed to vary with the physical properties of star-forming clouds. They run idealized chemo-dynamical simulations of star-forming galaxies in the mass range  $10^{10} - 10^{12} M_{\text{halo}}$  and vary the three IMF slopes of the Kroupa IMF in time following the results presented in Marks et al. (2012). The low-mass and intermediate mass slopes vary proportionally to  $[\text{Fe}/\text{H}]$  of the star-forming gas. The high-mass slope anticorrelates roughly log-linearly with the density of a high-density gaseous core where star formation occurs and correlates linearly with  $[\text{Fe}/\text{H}]$ .

They find that in strongly star-forming environments, high-density molecular gas clouds form. These drive the high-mass slope to smaller values (a more top-heavy IMF), which in turn increases the number of supernovae and the amount of feedback. Thus, the total SFR decreases with re-

spect to their universal IMF model. The increased supernova output sets the final metallicity and  $\alpha$ -enhancement above fiducial values.

This is similar to the observational results from [Clauwens et al. \(2016\)](#), who show that a metallicity-dependent IMF can speed up the quenching process. They maintain that a lack of feedback at late times will cause a last burst of star formation that empties the gas reservoir. While their study uses idealized simulations instead of the full cosmological context our of work, it is nevertheless instructive that our single parameter model shows opposite trends, where SFRs are increased in the varying model and total metallicity is decreased. The most apparent reason for this dissimilar result is that [Bekki \(2013\)](#) include a second parameter, the density dependence in his high-mass slope variation. This produces top-heavy IMFs even at later times when the metallicity has increased and would produce a bottom-heavy IMF in our model.

Also, [Recchi & Kroupa \(2015\)](#) study the IMF variation proposed by [Marks et al. \(2012\)](#) in the context of the IGIMF theory. To better match the mass-metallicity relation they include the SFR as a further parameter, which determines the exponent of the embedded cluster mass function. They conclude that any model that allows the IMF to be more top-heavy in more massive systems will be able to reproduce the mass-metallicity relation.

With accumulating observational and theoretical efforts in understanding possible IMF variations, it is becoming clearer that if an intrinsic IMF variability exists, its effect is to produce shallower high-mass slopes (or a more top-heavy IMF) at early times and evolve to become more bottom-heavy toward  $z = 0$  ([Davé 2008](#)). In our model this trend results directly from the fact that the total metallicity is a monotonically rising function with time. However, although the additional density parameter in [Bekki \(2013\)](#) produces a non-monotonic change of the IMF slope with time, it follows the SFH which drops towards  $z = 0$ . Given the variety of models attempting to study IMF variations, it is also clear that theoretical work has not yet converged on a consensus. But since the IMF is a fundamental parameter in many models of star and galaxy formation, any deviation from a universal shape will have far reaching consequences.

## 6 SUMMARY

The strength of energetic feedback from supernova and black holes is not well constrained by observations. Although simulations require some amount of feedback to control the runaway character of star formation and to match empirical relations such as the fundamental plane and the  $M_{\star} - M_{\text{crit},200}$  relation, the (sub-grid) parameter choices used in simulations cannot be determined from first principle calculations but rather rely on empirical input. Variable IMF models add additional complications here, because their effects can be degenerate with the feedback models themselves. Thus far, theoretical investigations have largely sidestepped this problem and focussed on constraining feedback under the assumption of a universal IMF, for simplicity.

In this study, we investigate the effects of a metallicity-dependent IMF that is constrained by observations of a sample of ETGs from the CALIFA survey. We have quantified

the differences exhibited by Milky Way analogues whose IMF varies with the total metallicity of the gas from which each star particle (representing a single stellar population) forms with respect to “standard” galaxies with a universal Chabrier IMF. We did not recalibrate the feedback strength or adjust any other parameters in the simulations, thus our results expose the effect of the variable IMF in isolation. This maximizes the corresponding effects and thus brackets the uncertainty due to a possible environmental dependence of the IMF.

One interesting outcome of our variable IMF model is that it produces too many stars to match the  $M_{\star} - M_{\text{crit},200}$  relation. This results from a slight change of the star formation history, generally being higher than the Chabrier model around  $z \sim 2 - 3$ . Late time SFRs vary between halos. Halos 9 and 28 show a slightly lower SFR compared to the Chabrier IMF in the last  $\sim 2$  Gyr. Whereas the SFR of Halo 6 does not significantly change and Halo 24 has  $\sim 0.5$  dex higher SFR since  $z \sim 0.3$  (compared to the Chabrier IMF halos).

The most significant result is that the metallicity evolution rises faster and flattens out early, which produces lower total metallicities. The MDF of stars is then less broad and more peaked. We have investigated the metal production further by examining the  $\alpha$ -abundance and its dependence on iron abundance. The corresponding distributions are broader in the variable IMF model, and even hint at a bimodality. To compare this accurately with observations, we mimic the selection function of stars in the APOGEE survey. This includes a spatial selection in the disk and in terms of the scale height. But since APOGEE observes primarily red clump stars, it also includes an age selection (see [Bovy et al. 2014](#)). The distribution in the  $[\alpha/\text{Fe}]$ - $[\text{Fe}/\text{H}]$  plane is strongly influenced by the IMF model, with the slope of the relation being much steeper in the variable model. This model in fact matches the APOGEE data considerably better, since its mean is closer to the observed values. Although the Chabrier model does not pass through the data, its slope appears closer the data, but its normalization is too high by 0.3 dex. Overall, these results highlight the significant constraining power in detailed abundance patterns for fundamental questions in galaxy formation such as the degree of universality of the stellar IMF. More detailed simulation studies will be needed to fully understand the non-linear cross-talk between feedback modelling, chemical enrichment, and the variability of the IMF.

## ACKNOWLEDGMENTS

We thank an anonymous referee for suggestions and constructive criticism which considerably improved the quality of this paper.

The authors also thank Robert Grand, Hans-Walter Rix and Rüdiger Pakmor for useful conversation. TAG and VS acknowledge funding through the Collaborative Research Centre SFB 881 “The Milky Way System” (subproject A1) of the German Research Foundation (DFG). This research was carried out on the High Performance Computing resources of the DRACO cluster at the Max Planck Computing and Data Facility (MPCDF) in Garching operated by the Max Planck Society (MPG).



## REFERENCES

- Bastian N., Covey K. R., Meyer M. R., 2010, *ARA&A*, **48**, 339
- Bastian N., Covey K. R., Meyer M. R., 2011, in Johns-Krull C., Browning M. K., West A. A., eds, *Astronomical Society of the Pacific Conference Series Vol. 448, 16th Cambridge Workshop on Cool Stars, Stellar Systems, and the Sun*. p. 361 ([arXiv:1011.6512](#))
- Bekki K., 2013, *MNRAS*, **436**, 2254
- Blancato K., Genel S., Bryan G., 2017, *ApJ*, **845**, 136
- Bovy J., et al., 2014, *ApJ*, **790**, 127
- Bruzual G., Charlot S., 2003, *MNRAS*, **344**, 1000
- Cappellari M., et al., 2013, *MNRAS*, **432**, 1862
- Chabrier G., 2003, *PASP*, **115**, 763
- Chabrier G., Hennebelle P., Charlot S., 2014, *ApJ*, **796**, 75
- Clauwens B., Schaye J., Franx M., 2016, *MNRAS*, **462**, 2832
- Conroy C., van Dokkum P. G., 2012, *ApJ*, **760**, 71
- Conroy C., Dutton A. A., Graves G. J., Mendel J. T., van Dokkum P. G., 2013, *ApJ*, **776**, L26
- Davé R., 2008, *MNRAS*, **385**, 147
- Doherty C. L., Gil-Pons P., Lau H. H. B., Lattanzio J. C., Siess L., Campbell S. W., 2014, *MNRAS*, **441**, 582
- Dutton A. A., et al., 2011, *MNRAS*, **416**, 322
- Few C. G., Courty S., Gibson B. K., Michel-Dansac L., Calura F., 2014, *MNRAS*, **444**, 3845
- Fishlock C. K., Karakas A. I., Lugaro M., Yong D., 2014, *ApJ*, **797**, 44
- Gallazzi A., Charlot S., Brinchmann J., White S. D. M., Tremonti C. A., 2005, *MNRAS*, **362**, 41
- Grand R. J. J., et al., 2017a, preprint, ([arXiv:1708.07834](#))
- Grand R. J. J., et al., 2017b, *MNRAS*, **467**, 179
- Gunawardhana M. L. P., et al., 2011, *MNRAS*, **415**, 1647
- Guszejnov D., Hopkins P. F., Ma X., 2017, preprint, ([arXiv:1702.04431](#))
- Hopkins P. F., 2013, *MNRAS*, **433**, 170
- Hoversten E. A., Glazebrook K., 2008, *ApJ*, **675**, 163
- Karakas A. I., 2010, *MNRAS*, **403**, 1413
- Kirby E. N., et al., 2010, *ApJS*, **191**, 352
- Kirk H., Myers P. C., 2011, *ApJ*, **727**, 64
- Kobayashi C., Umeda H., Nomoto K., Tominaga N., Ohkubo T., 2006, *ApJ*, **653**, 1145
- Kroupa P., 2001, *MNRAS*, **322**, 231
- Kroupa P., 2002, *Science*, **295**, 82
- Kroupa P., Weidner C., 2003, *ApJ*, **598**, 1076
- Kroupa P., Tout C. A., Gilmore G., 1993, *MNRAS*, **262**, 545
- Kroupa P., Theis C., Boily C. M., 2005, *A&A*, **431**, 517
- La Barbera F., Ferreras I., Vazdekis A., de la Rosa I. G., de Carvalho R. R., Trevisan M., Falcón-Barroso J., Ricciardelli E., 2013, *MNRAS*, **433**, 3017
- Lada C. J., Lada E. A., 2003, *ARA&A*, **41**, 57
- Larson R. B., 1998, *MNRAS*, **301**, 569
- Marinacci F., Pakmor R., Springel V., Simpson C. M., 2014, *MNRAS*, **442**, 3745
- Marks M., Kroupa P., Dabringhausen J., Pawłowski M. S., 2012, *MNRAS*, **422**, 2246
- Martín-Navarro I., et al., 2015, *ApJ*, **806**, L31
- Megeath S. T., et al., 2016, *AJ*, **151**, 5
- Meurer G. R., et al., 2009, *ApJ*, **695**, 765
- Mollá M., Cavichia O., Gavilán M., Gibson B. K., 2015, *MNRAS*, **451**, 3693
- Naiman J. P., et al., 2017, preprint, ([arXiv:1707.03401](#))
- Ness M., et al., 2017, preprint, ([arXiv:1701.07829](#))
- Nomoto K., Iwamoto K., Nakasato N., Thielemann F.-K., Brachwitz F., Tsujimoto T., Kubo Y., Kishimoto N., 1997, *Nuclear Physics A*, **621**, 467
- Pillepich A., et al., 2017, preprint, ([arXiv:1703.02970](#))
- Planck Collaboration et al., 2016, *A&A*, **594**, A16
- Portinari L., Chiosi C., Bressan A., 1998, *A&A*, **334**, 505
- Recchi S., Kroupa P., 2015, *MNRAS*, **446**, 4168
- Salpeter E. E., 1955, *ApJ*, **121**, 161
- Scalo J. M., 1986, *Fundamentals Cosmic Phys.*, **11**, 1
- Spiniello C., Trager S., Koopmans L. V. E., Conroy C., 2014, *MNRAS*, **438**, 1483
- Springel V., 2010, *MNRAS*, **401**, 791
- Vazdekis A., Casuso E., Peletier R. F., Beckman J. E., 1996, *ApJS*, **106**, 307
- Vogelsberger M., Genel S., Sijacki D., Torrey P., Springel V., Hernquist L., 2013, *MNRAS*, **436**, 3031
- Weisz D. R., et al., 2015, *ApJ*, **806**, 198
- Yan Z., Jerabkova T., Kroupa P., 2017, preprint, ([arXiv:1707.04260](#))

This paper has been typeset from a  $\text{\TeX}/\text{\LaTeX}$  file prepared by the author.